NASA/CR-1998 207314

N/S

IN-02-CR

067620

AIAA-98-0701
Reynolds-Averaged Navier-Stokes Simulations of Two Partial-Span Flap Wing Experiments

M.A. Takallu
Lockheed Martin Engineering & Sciences Company
Hampton, Virgina

K.R. Laflin
National Research Council
Hampton, Virginia

36th Aerospace Sciences Meeting & Exhibit
January 12–15, 1998 / Reno, NV

REYNOLDS-AVERAGED NAVIER-STOKES SIMULATIONS OF TWO PARTIAL-SPAN FLAP WING EXPERIMENTS

M.A. Takallu*
Lockheed Martin Engineering & Sciences Company
Hampton, VA

Kelly R. Laflin[†]
National Research Council
Hampton, VA

Abstract

Structured Reynolds Averaged Navier-Stokes simulations of two partial-span flap wing experiments were performed. The high-lift aerodynamic and aeroacoustic wind-tunnel experiments were conducted at both the NASA Ames 7- by 10-Foot Wind Tunnel and at the NASA Langley Quiet Flow Facility. The purpose of these tests was to accurately document the acoustic and aerodynamic characteristics associated with the principle airframe noise sources, including flap side-edge noise. Specific measurements were taken that can be used to validate analytic and computational models of the noise sources and associated aerodynamics for configurations and conditions approximating flight for transport aircraft. The numerical results are used to both calibrate a widely used CFD code, CFL3D, and to obtain details of flap side-edge flow features not discernible from experimental observations. Both experimental set-ups were numerically modeled by using multiple block structured grids. Various turbulence models, grid block-interface interaction methods and grid topologies were implemented. Numerical results of both simulations are in excellent agreement with experimental measurements and flow-visualization observations. The flow field in the flap-edge region was adequately resolved to discern some crucial information about the flow physics and to substantiate the merger of the two vortical structures. As a result of these investigations, airframe noise modelers have proposed various simplified models which use the results obtained from the steady-state computations as input.

Introduction

An aerodynamic challenge related to the design of subsonic transport aircraft is the determination and reduction of radiated airframe noise. Research[1] indicates that, as aircraft engines become quieter in the near future, a significant contributor to airframe noise of an aircraft on approach will be the high-lift system. Within the complex three-dimensional flow field of a high-lift system, the side-edge region of a partial-span flap is suspected to produce the dominant noise source.[2] The noise associated with this region is believed to be due to the formation and shedding of a flap side-edge vortex and its interaction with the free shear layer. Although the general mechanisms of flap side-edge vortex formation are well known, details of the flow field physics and associated unsteadiness required for noise source generation in the flap side-edge region are not completely understood. Knowledge of these details, as well as other details of high-lift flow fields, are crucial to the design of improved high-lift systems with reduced airframe noise levels. Required flow field details, that are not discernible from experimental measurements or observations, will likely be determined through the use of computational fluid dynamics (CFD).

Noise generation is an unsteady phenomenon, but unsteady viscous three-dimensional flow field computations are both time consuming and expensive. For this reason, airframe noise modelers have proposed various simplified models which use the results obtained from steady-state Reynolds Averaged Navier-Stokes (RANS) computations as input for noise source models.[3-4] However, before the RANS results can be confidently used in this capacity, they must be calibrated against reliable test data.

In this paper, experimental results of two partial-span flap wing experiments are used to calibrate the use of a RANS flow solver for predicting high-lift flow fields and providing the details required by airframe noise models. Although, Jones *et al*[5] have demonstrated

---

*Supervisor, Aerodynamics Section
NASA Langley Program Office. Associate Fellow AIAA.
m.a.takallu@larc.nasa.gov
[†]Resident Research Associate, Aero and Gas Dynamics
Division, NASA Langley Research Center. Non-Member.
k.r.laflin@larc.nasa.gov

the ability of such a flow solver to simulate flow fields about two-dimensional and three-dimensional multi-element high-lift configurations, it is not known if RANS flow solvers are capable of providing the small-scale aerodynamic details associated with airframe noise sources.[6] In the present work, structured RANS computations were used as a modern analysis tool to study two high-lift aerodynamic and aeroacoustic wind-tunnel experiments in order to both calibrate a widely used CFD code and to simulate some of the flow features not captured by the experiments. Therefore, a brief discussion of the two NASA experiments is followed by a description of the numerical strategy. Computed results, that concentrate on the flap side-edge region, will be presented in detail and compared with experimental data.

Experimental Investigations

A series of partial-span flap wing wind-tunnel experiments were conducted at both the NASA Ames Research Center 7- by 10-Foot Wind Tunnel[7] (7×10) and at the NASA Langley Quiet Flow Facility[8] (QFF). The purpose of these tests was to accurately document the acoustic and aerodynamic characteristics associated with the principle airframe noise sources, including flap side-edge noise. Specific measurements were taken that can be used to validate analytic and computational models of the noise sources and associated aerodynamics for configurations and conditions approximating flight for transport aircraft.

7×10 Experiment

The NASA Ames 7×10 test provided a data base of aerodynamic forces and moments with accompanying wing pressure distributions (750 pressure taps) for a partial-span flap wing model[7]. A sketch of the model set-up is shown in Figure 1. The model was designed so that a constant-chord rectangular wing with a NACA 63_2-215 Mod B airfoil cross-section resulted when the flap was retracted; thereby providing a reference "two-dimensional" flow to which the three-dimensional flows of deployed-flap configurations could be compared. The wing chord and span are c_w=30 inches and 2.5 c_w, respectively. The half-span flap has a chord of $0.3c_w$. Measurements were taken at angles of attack ranging from 0 to 15 degrees with flap deflections of 29 and 39 degrees. Microphone array and 7-hole probe near wake surveys where also conducted as part of the 7×10 test.

QFF Experiment

In an effort complementary to the 7×10 test, aerodynamic and noise issues were investigated at the QFF using a 16 inch chord model of similar geometry to that of the 7×10 test model but with an aspect ratio of 2.25. In the QFF (Figure 2), jet flow enters vertically through the floor of an anechoic chamber via a converging inlet nozzle which accelerates the jet flow to the desired entrance conditions. The partial-span flap model (Figure 3) is mounted between two rectangular-shaped end plates and positioned in the vertical jet (Figure 4). The jet is constrained in the spanwise direction of the wing by the two end plates but is otherwise allowed to expand. Flow exits through a converging exhaust nozzle positioned at the ceiling of the large anechoic chamber. Because of the expansion of the jet flow between the two end plates, wing loading measurements were lower than those of the 7×10 test for similar angles of attack and flap-deflection angles. Therefore, the angles of attack of the QFF experiment were adjusted so that the wing loadings more closely matched those obtained in the Ames test. Microphone arrays, directional microphones, 5-hole probe wake surveys, pressure sensitive paint (PSP) applications, and laser light sheet flow visualization were employed as part of the QFF test.

Numerical Approach

All computations were performed on the Cray C-90 and Cray Y-MP super-computers of the National Aerodynamic Simulation (NAS) facility located at the NASA Ames Research Center.

Flow Solver

The RANS flow solver CFL3D[9] was used to simulate both the 7×10 and the QFF experiments. This code uses the unsteady, three-dimensional, compressible, thin-layer Navier-Stokes equations to model the flow on body-fitted structured grids with multiple-block topologies. It is a semi-discrete cell-centered finite-volume scheme, that can make use of grid sequencing, local time-stepping, and multigridding to accelerate convergence to a steady state; all three techniques were utilized for all computations presented herein. CFL3D allows both C0-continuous (one-to-one matching at block interfaces) and patched block interfaces; both of these were used in this study.

CFL3D advances the solution using an implicit approximate factorization (AF) scheme. A block tridiagonal inversion results for each AF sweep by using

first-order accurate upwind-biased differencing to approximate the implicit spatial derivatives. However, because steady state solutions are considered, flux-difference splitting (FDS) can be used in conjunction with a diagonal scheme to require only a scalar tridiagonal inversion for each AF sweep. This simplification reduces both the required memory and CPU time without decreasing the accuracy of the computations. CFL3D can also employ flux-vector splitting, but this option was not used to perform the computations presented here. Explicit spatial derivatives are approximated using third-order accurate upwind-biased differencing for the inviscid terms and second-order accurate centered differencing for the viscous terms. Fully turbulent solutions were obtained using the Spalart-Allmaras[10] one-equation turbulence models. The Spalart-Allmaras turbulence model is often employed when high-lift configurations are considered because it has been performing adequately for multiple solid surfaces and wake/boundary layer interactions. In addition, it seems to produce more accurate solutions in reverse flow regions, as compared with other turbulence models.

For patched zones, data transfer between zones is accomplished by linear interpolation in the computational coordinate system. The interpolation coefficients required for CFL3D are obtained as a pre-processing step using the RONNIE[9] preprocessor.

Gridding Strategy

Since these computed high-lift flow fields are to be directly compared with experimental measurements and observations, it is logical, as demonstrated by Cao et al[11] that the wind tunnel walls need to be modeled as part of the numerical simulation. The multiple components of a high-lift system require multiple grid blocks. As it was mentioned earlier, CFL3D allows both C0-continuous (one-to-one matching at block interfaces) and patched block interfaces; both of these were used in this study. The addition of the rectangular walls adds some difficulty to a C0-continuous grid construction, especially when the test facility geometry is complex, such as the geometry of the QFF. An alternative to C0-continuous grid construction is to use patched block interfaces. By using patched grids, the grid construction procedure is simplified and the required number of grid points can generally be reduced. In order to substantiate the use of patched grid interfaces in future studies, computations where performed on both C0-continuous and patched grids and the resulting solutions where compared to the experimental data.

Numerical Simulation of 7x10 Experiment

The partial-span flap wing tested in the NASA Ames 7x10 was modeled using both a 16-block grid with C0-continuous interfaces (Figure 5) and a 19-block grid with mixed C0-continuous and patched interfaces (Figure 6). The 16-block and 19-block grids have a total of approximately 2.3 and 2.6 million points, respectively. In each grid, the constant-area rectangular test section was extended 15 chord lengths upstream and downstream from the wing. Wing angles of attack of 4, 8, and 10 degrees with a flap deflection of 29 degrees were considered for the numerical simulations. The Reynolds number and Mach number used for the simulations were 3.6×10^6 and 0.2, respectively; matching the 7×10 test conditions. The computational grids used viscous grid spacing suitable for turbulent boundary-layer computations at all wing surfaces. In addition, a high concentration of grid-points was used to resolve the flow field about the flap side-edge. Inviscid grid-points spacing was used at all solid surfaces, apart from those of the wing components, to limit the total number of grid points and, thus, the required memory and CPU time of the simulations. This methodology was successfully used by other researchers to compute the above set-up both with structured[6] and unstructured grids.[12]

Numerical Simulation of QFF Experiment

When a constant area rectangular-shaped test section is considered, the grid generation, boundary-condition specification and computations for a numerical simulation are relatively simple; this is the case for the numerical simulation of the 7×10 experiment. However, numerical simulations of the QFF experiment present several challenges that have not been previously addressed for the calculation of three-dimensional, viscous, high-lift flow simulations. These challenges include the numerical simulation of a high-lift device in a semi-constrained jet flow, the presence of large-scale circulatory flow throughout a large test chamber, and the existence of large regions of near-stagnant flow which is known to cause convergence and accuracy difficulties for compressible codes.[13] A series of grid alterations, such as grid refinements around the end-plates and inside the area representing the anechoic room, were performed to meet these computational challenges.

The QFF experimental set-up was modeled using a 21-blocked grid with C0-continuous interfaces having approximately 3.2 million grid points (Figure 7). As illustrated in Figure 7a and 7b, the first 12 grid blocks

used in the inner-blocks of the 7x10 grid were utilized also as the inner-blocks of the QFF grid. These blocks simulate the wing/flap system and the space between the supporting end-plates. Figure 7c shows the 21-block QFF grid. For ease of illustration, each block is colored differently.

The chord Reynold's number and average inlet-throat Mach number are 1.8×10^6 and 0.2, respectively. To achieve the correct throat Mach number, the pressure ratios at the inlet nozzle and exhaust exit boundaries are adjusted iteratively.

Even though the numerical simulation of the QFF experiments included computations of a three element high-lift configuration composed of a wing, partial-spanned flap and a full-span leading edge slat, the results presented in the following will be related to the two-element configuration only[14]. In addition to CFL3D, another widely used Langley RANS code, TLNS3D-MB[15] was also utilized to simulate the QFF experiment.[14] Both grid methodologies, grid blocks with C0-continuous block boundaries and patched block interfaces, were utilized. Also, various angles-of-attack and flap deflections were computed. However, for brevity only results of the computations using CFL3D code and the 21 block grid with C0-continuous grid block boundaries for the angle-of-attack of 16 degrees and 29 degree flap-deflection are presented.

Results
All numerical simulations of the experimental test cases have been completed and show excellent agreement with the experimental data. Various grid sizes and topologies along with various turbulence models were computed. A wide range of wing angle of attack and flap deflections were also analyzed. Some sample results are presented. These results (Figures 8-18) will focus on the validation of the converged numerical solutions through comparisons with experimental data and on the analysis of the three-dimensionality of the high-lift flow field. The analysis will concentrate on the flow field in the flap side-edge region.

7×10 Simulation
Figure 8 gives the convergence history for the 10 degree angle-of-attack. Solution convergence of this turbulent-viscous simulation is reached within 3000 iterations, with a four-order drop in the residual magnitude. Both multigridding and mesh sequencing were used to increase the solution convergence rate.

Figure 9 compares the computational and experimental surface pressure distributions at four spanwise locations. Two of the spanwise stations are in the flapped region of the wing and the other two are in the non-flapped segment of the wing. As is shown, the computations are in good agreement with the experimental data. The saddle type sectional pressure profile near the flap side-edge is an indication of the existence of some vorticity generation in this region. In fact a detailed analysis of the flow field at the flap side edge reveals the (see Figures 10 and 11) merging of a strong vortex at the lower (pressure) side of the flap edge with a weaker vortex from the top (suction) side. Figure 10 shows the surface pressure contour and the extent of the flow disturbance due to the flap on both flapped region and non-flapped segment of the wing.

Figure 12 presents flap side-edge total pressure contours and grid topologies for both the 16-block grid with CO-continuous grid boundaries and the 19-block grid with patched block boundaries. Despite the differences in grid topologies and grid-point concentrations, both numerical solutions produce agreeable results. This fact indicates some grid-insensitivity of the present numerical solutions in the flap side-edge region.

QFF Simulation
As it is shown in Figure 13a, the Mach contour on a cutting plane through the mid-span of the tunnel illustrates the turning of the flow towards the flap trailing edge. The turning phenomenon is much stronger for the QFF set-up than those observed for the 7x10 simulation and could be explained by the lack of confining walls on the top and bottom of the wing set-up. This can affect the down stream location and shedding of the merged flap side-edge vortex. Figure 13b shows a portion of the QFF experiment configuration and grid geometry downstream of the nozzle looking onto the suction side of the wing. Streamlines in the figure illustrate the extent of the downwash that results from the semi-constrained jet.

Figures 14 and 15 show pressure contours on the flap side-edge and in several planar cuts normal to the stream direction. Note that the flap side-edge surface pressure patterns are similar to those of the 7×10 simulation (Figure 10). This is another indication that the QFF simulation can adequately capture some of the flow phenomena of particular interest to the acoustics community. As mentioned earlier, the appearance and merging of the vortices at the flap side-edge has been suspected to be one of the major sources of airframe

noise.

Figure 15 gives planar cuts normal to the flap side-edge at various chord locations. The positions of these cuts are indicated in Figure15f. The pressure contour lines show details of developing vortical structures and indicates that the flap side-edge flow of the QFF simulation is well resolved.

Both the NASA Ames 7x10 and the NASA Langley QFF experiment simulations show the development and merger of a weak and a strong vortex in the flap side-edge region. In each case, a strong vortex develops as a result of flow separation from the lower surface at the flap edge (Figure 15f). Flow reattachment associated with this vortex occurs on the flap edge. This attached flow separates at the upper surface of the flap and forms a weaker vortex along the flap upper surface (Figure 15b). Eventually, the reattachment position of the strong vortex exceeds the confines of the flap edge (Figure 15c) and the two vortices merge into a single vortex (Figure 15d). The vortex detaches at the flap trailing edge (Figure 15e).

These computed results are consistent with laser-light sheet, surface pressure measurements[16] and pressure-sensitive paint (PSP) flow visualization observations[17] conducted during the QFF experiment. Comparisons of the computed results with experimental (PSP) observations on the top and flap side-edge are shown in figure 16 and figure 17, respectively.

Figure 18 compares the computational and experimental surface pressure distributions at six spanwise locations. Four of the spanwise stations are in the flapped region of the wing and the other two are in the non-flapped region of the wing. As is shown, the computations are in good agreement with the experimental data. Figures 18c and 18d show the signature of the flap side-edge vortex on these two section pressure profiles. An in-depth look at the areas enclosed by the pressure distributions indicates the extent of the span loading for the set-up discussed above.

Summary

Numerical simulations of two partial-span flap wing experiments have been successfully completed. These three-dimensional steady-state Reynolds-averaged Navier-Stokes simulations involved the modeling of two partial-span high-lift wings, including the wind tunnel walls, mounted in two different test facilities: the NASA Ames 7- by 10-Foot Wind Tunnel and the NASA Langley Quiet Flow Facility. Numerical simulation of the QFF experiment which consisted of modeling of the high-lift wing, end-plates, inlet nozzle, anechoic room and exhaust nozzle, presented several challenges that were successfully addressed for the first time in this work. Various turbulence models, grid block-interface interaction methods and grid topologies were implemented. The flow field in the flap side-edge region was adequately resolved to discern some crucial information about the flow physics and to substantiate the merger of the two vortical structures. Numerical results of both simulations are in excellent agreement with experimental measurements and flow-visualization observations.

Acknowledgments

References

[1]Hardin, J.C., "Airframe Self-noise - Four Years of Research'" NASA TM X-73908, 1976.

[2]Revel, J.D., "The Calculation of Aerodynamic Noise Generated by Large Aircraft at Landing Approach," Paper JJ9, 87th Meeting, Acoustical Society of America, April 1974.

[3]Khorrami, M.R., Singer, B.A. and Takallu, M.A., "Analysis of Flap Side-Edge Flow Field for Identification and Modeling of Possible Noise Sources," SAE Paper No. 971917, presented at the 1997 SAE Noise and Vibration Conference and Exposition, Grand Traverse, MI, May 1997.

[4]Steett, C.L. "DNS of Flap-Edge Flowfield Instabilities," proceedings of the Airframe Noise Workshop, Long Beach, California, 11-12 June 1997.

[5]Jones, K.M., Biedron, R.T., and Whitlock, M., "Application of a Navier-Stokes Solver to the Analysis of Multielement Airfoils and Wings Using Multizonal Grid Techniques," AIAA Paper 95-1855, 1995.

[6]Mathias, D.L., Roth, K.R., Ross, J.C., Rogers, S.E., and Cummings, R.M., "Navier-Stokes Analysis of the Flow About a Flap Edge," AIAA Paper 95-0185, 1995.

[7]Storms, B.L., Takahashi, T.T., and Ross, J.C., "Aerodynamic Influence of a Finite-Span Flap on a Simple Wing," SAE paper no. 95-1977, presented at SAE Aerotech '95, Los Angeles, CA, September 1995.

[8]Hubbart, H.H. and Manning, J.C., "Aeroacoustic Research Facilities at NASA Langley Research Center'" NASA TM 84585, March 1983.

[9]Krist, S.L., Biedron, R.T., and Rumsey, C.L., "CFL3D User's Manual (Version 5.0)," Aerodynamic and Acoustic Methods Branch, NASA Langley Research Center, 1996.

[10]Spalart, P. and Allmaras, S., "A One-Equation Turbulence Model for Aerodynamic Flows," AIAA 92-0439, 1992.

[11]Cao, H., Kusunose, K., Spalar, P., Ishimitsu, K., Rogers, S., and McGhee, R., "Study of Wind Tunnel Wall Interference for Multi-Element Airfoils Using a Navier-Stokes Code," AIAA Paper 94-1993, June 1994.

[12]Anderson, W.K., Rausch, R.D., and Bonhaus, D.L., "Implicit/Multigrid Algorithms for Incompressible Turbulent Flows on Unstructured Grids," AIAA 95-1740, 1995.

[13]Volpe, G., "On the Use and Accuracy of Compressible Flow Codes at Low Mach Numbers," AIAA 91-1662, 1991.

[14]Takallu, M.A.,"Reynolds-Averaged Navier-Stokes Simulations of Two Partial-Span flap Wing Experiments", proceedings of the Airframe Noise Workshop, Long Beach, California, 11-12 June 1997.

[15]Vatsa, V.N., Sanetrik, M.D., Parlette, E.B., Eiseman, P., and Cheng, Z., "Multi-block Structured Grid Approach for Solving Flows over Complex Aerodynamic Configurations," AIAA 94-0655, 1994.

[16]Meadows, K.R., Brooks, T.F., Humphreys, W.M., Hunter, W.H., and Gerhold, C.H., "Aeroacoustic Measurements of a Wing-Flap Configurations," AIAA 97-1595, 1997.

[17]Radeztsky, Jr., R.R., "Experimental Measurements of the Flap-Edge Flowfield," proceedings of the Airframe Noise Workshop, Long Beach, California, 11-12 June 1997.
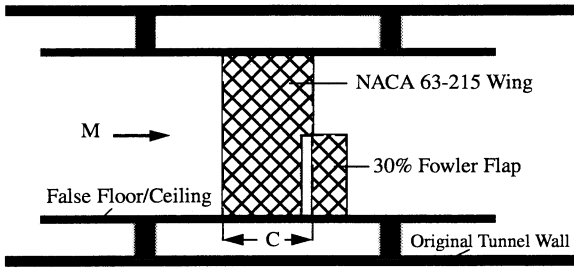
Figure 1: Sketch of the side view of the Ames 7×10 experimental set-up.
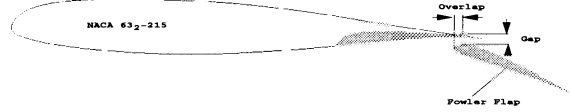
Figure 3: Sketch of the high-lift wing section, a planar cut at wing mid-span.
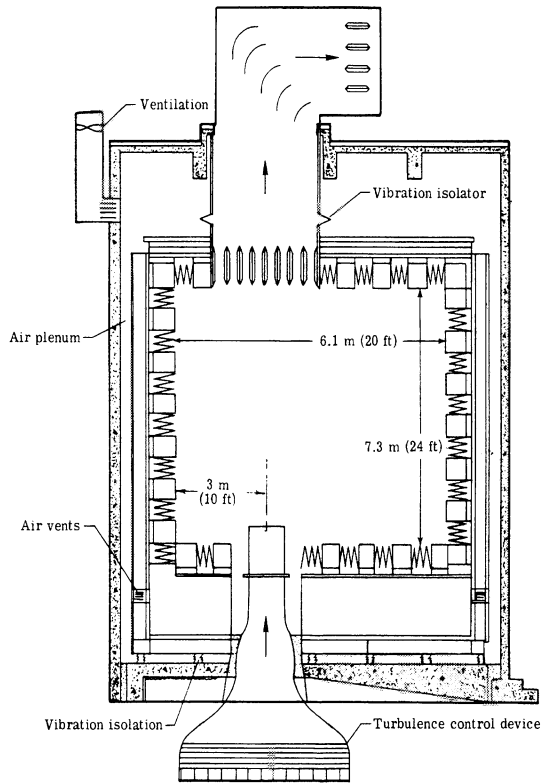
Figure 2: Diagram of the LaRC Quiet Flow Facility
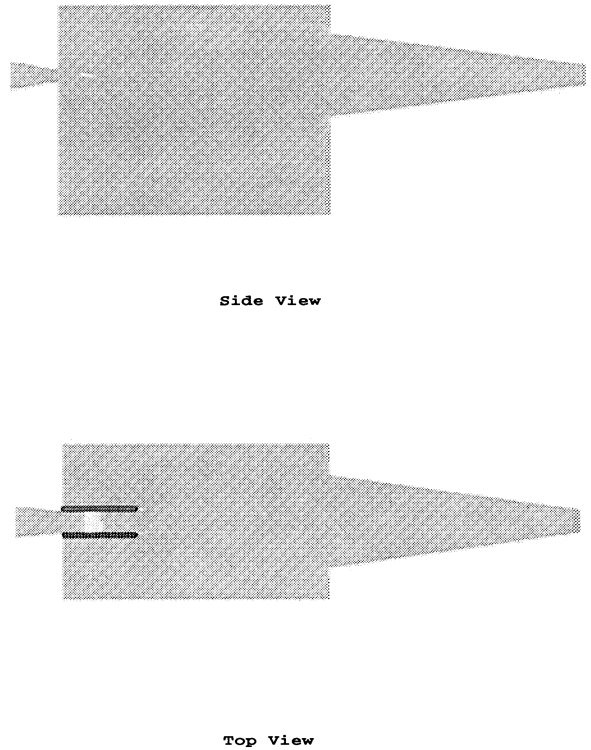
Figure 4: Top- and side-view of QFF set-up.

American Institute of Aeronautics and Astronautics
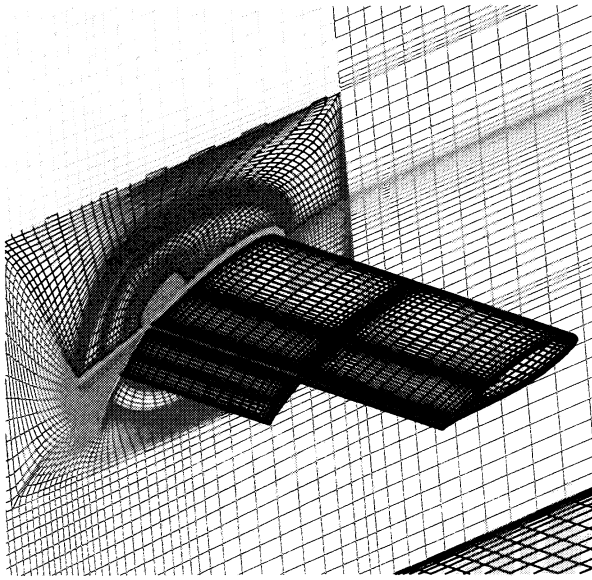
Figure 5: Grid blocks with C0 continuous block interfaces for 16-block "7x10 grid".
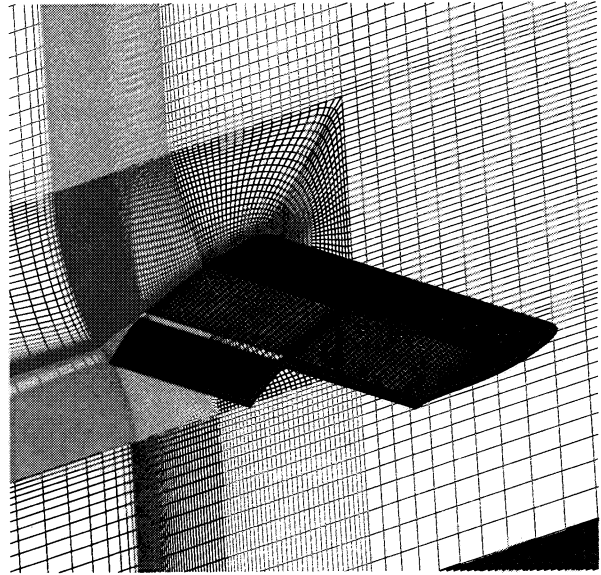
Figure 6: Grid blocks with patched block interfaces for 19-block "7x10 grid".
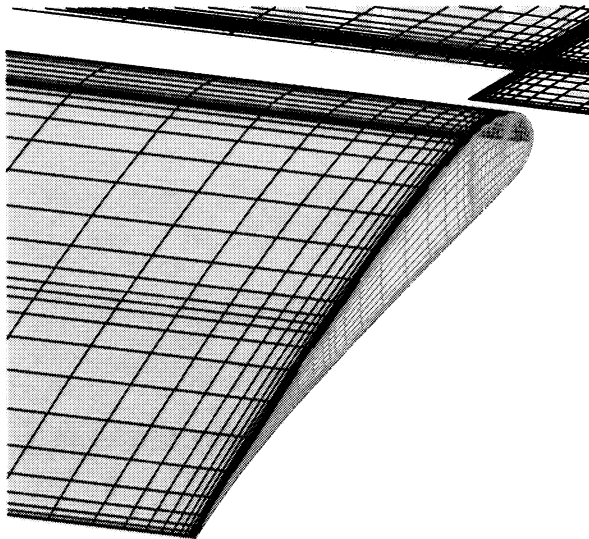
Figure 5b: Close-up view of the flap side-edge grid with C0 continuous block interfaces.
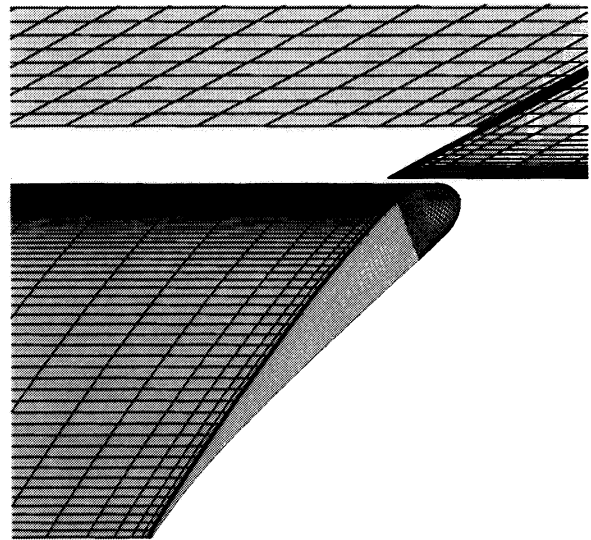
Figure 6b: Close-up view of the flap side edge grid with patched block interfaces.
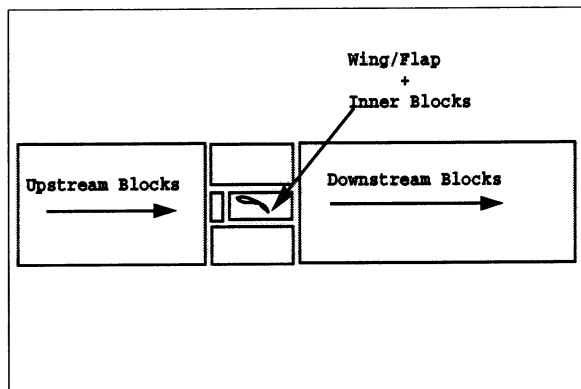
Figure 7a: Sketch of "7x10 grid" blocks versus "QFF grid" blocks below.
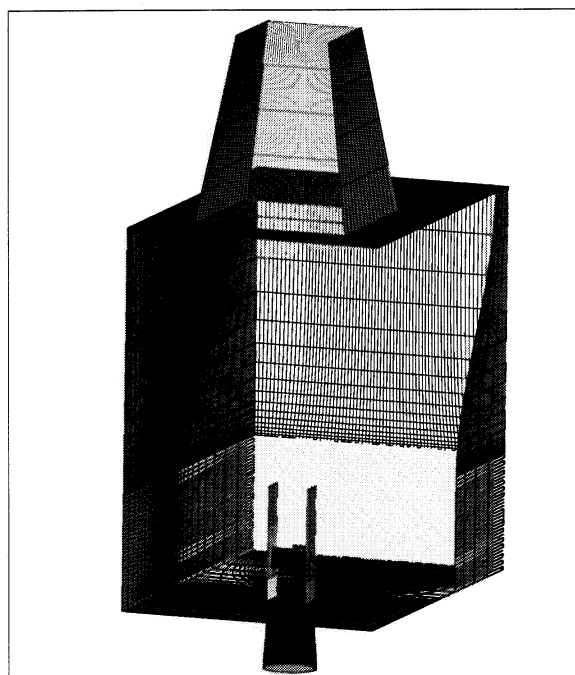
Figure 7c: Close-up view of the "QFF grid" topology between the supporting end-plates.
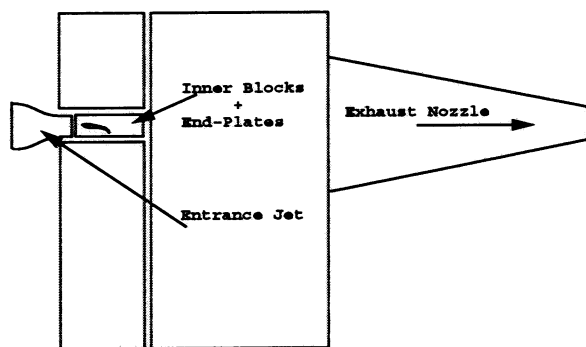
Figure 7b: Sketch of "QFF grid" blocks using the inner block of "7x10 grid" blocks.
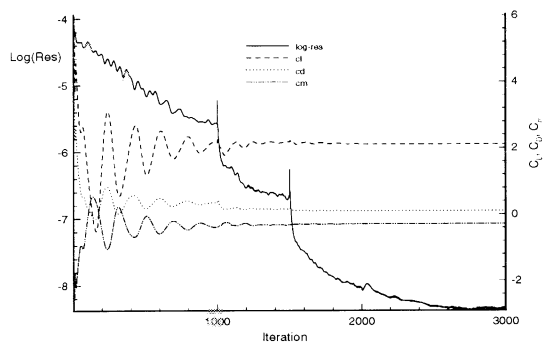
Figure 8: Convergence history for "7x10 simulation", M=0.2, Re=3.6×10^6, α=10°, δ_f=29°.
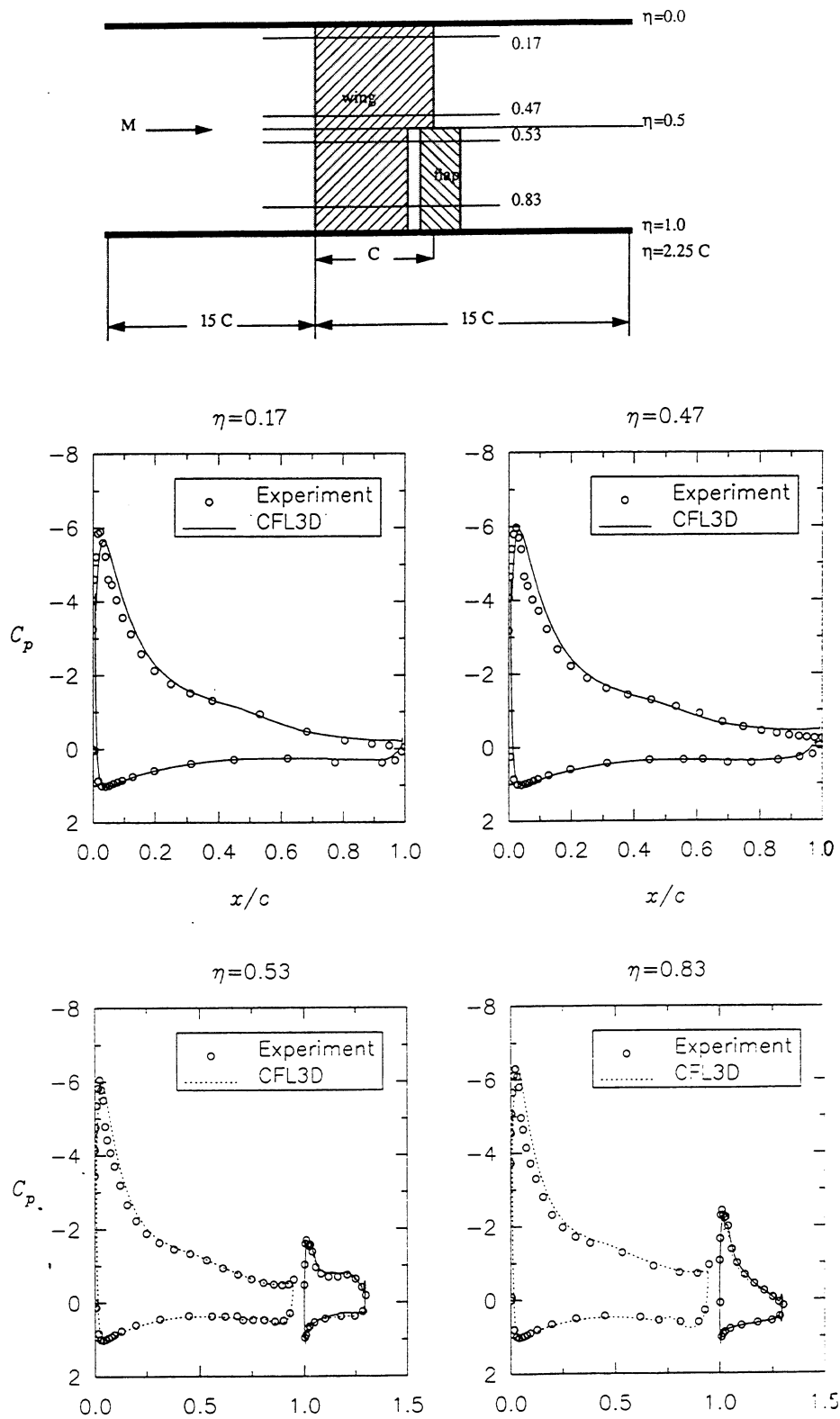
Figure 9: Comparison of computed pressure distributions at various spanwise locations with the "7×10 data"

$M=0.2, Re=3.6×10^6, \alpha=10°, \delta_f=29°$
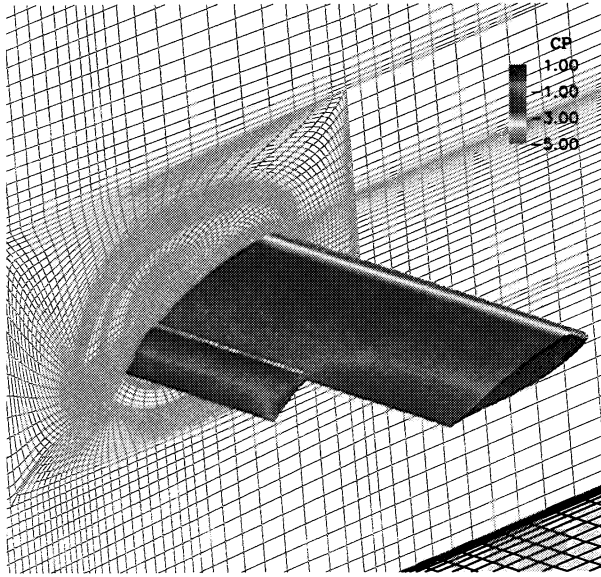
Figure 10: Surface pressure coefficient contour and "7x10 grid" topology of the tunnel side wall, M=0.2, Re=3.6×10^6, α=10°, δ$_f$=29°.
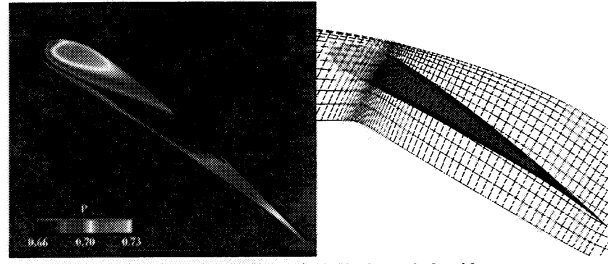
Flap-Edge Contour of 19-Block Patched Grid
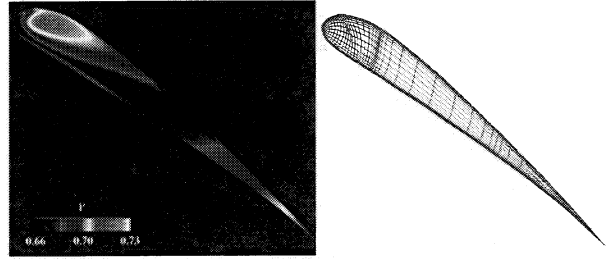
Flap-Edge Contour of 16-Block One-to-One Matched Grid

Figure 12: Comparison of flap side-edge pressure contours for the two different grid block systems and topologies, M=0.2, Re=3.6×10^6, α=10°, δ$_f$=29°.

P
0.73
0.71
0.70
0.68
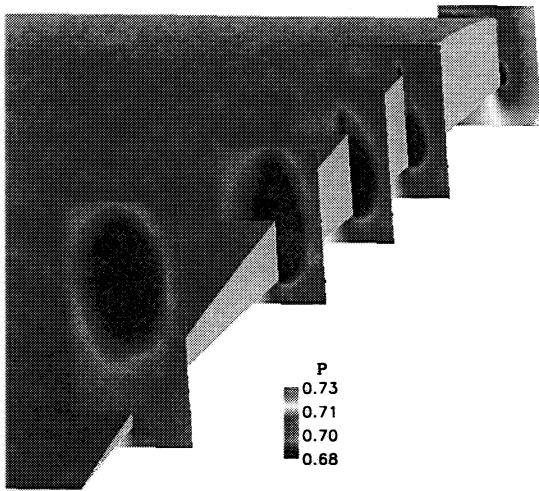
Figure 11: 7x10 pressure contour at and on a perpendicular cut to the flap side-edge, M=0.2, Re=3.6×10^6, α=10°, δ$_f$=29°.

M
0.41
0.27
0.14
0.00
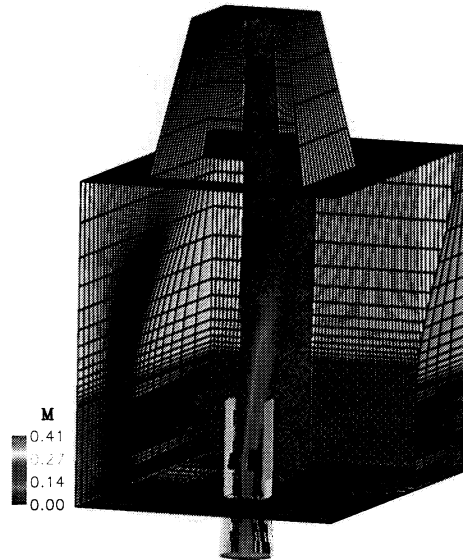
Figure 13a: Grid topology of QFF and Mach contour in a planar cut at the mid-span, M=0.2, Re=1.8×10^6, α=16°, δ$_f$=29°.

11
American Institute of Aeronautics and Astronautics
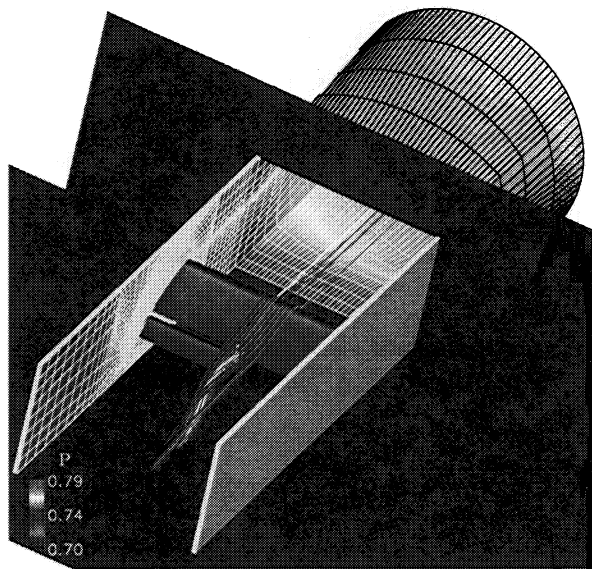
Figure 13b: Close-up view of pressure contour and stream lines near the jet nozzle for the "QFF simulation", M=0.2, Re=1.8×10^6, α=16°, δ$_f$=29°.
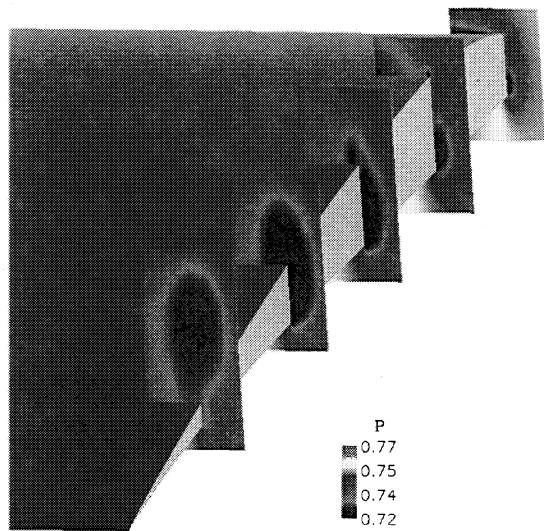
Figure 14: Close-up view of pressure contours in planar cuts perpendicular to the flap side-edge for the "QFF simulation", M=0.2, Re=1.8×10^6, α=16°, δ$_f$=29°.
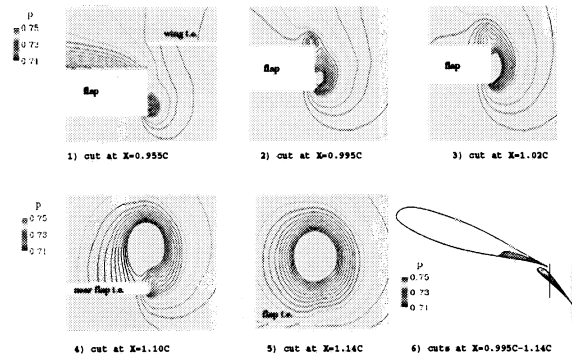
Figure 15: Pressure contour lines on various cutting planes perpendicular to flap side-edge for the "QFF simulation", M=0.2, Re=1.8×10^6, α=16°, δ$_f$=29°.
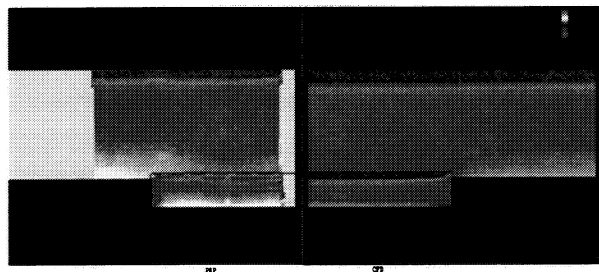
Figure 16: Comparison of PSP and CFD pressure coefficients on the suction side of the wing for the "QFF simulation", M=0.2, Re=1.8×10^6, α=16°, δ$_f$=29°.
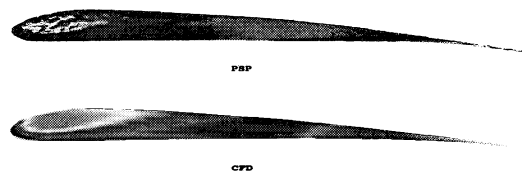
Figure 17: Comparison of PSP and CFD pressure coefficients on the flap side-edge for the "QFF simulation", M=0.2, Re=1.8×10^6, α=16°, δ$_f$=29°.
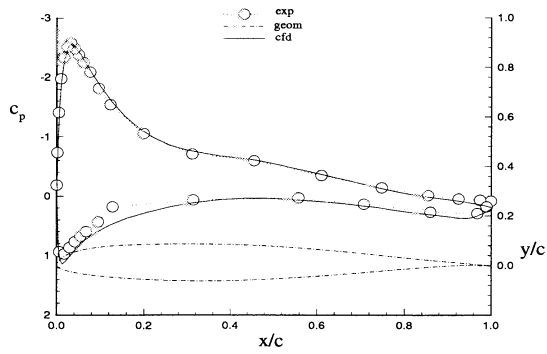
a) Cut at 0.25 span-station
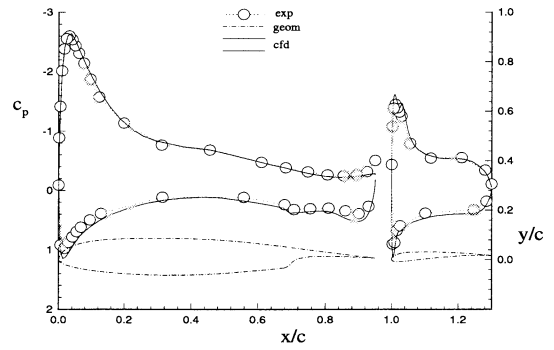
d) Cut at 0.528 span-station, near flap side-edge.

b) Cut at 0.4722 span-station, near flap side-edge.

e) Cut at 0.5833 span-station

c) Cut at 0.5028 span-station, near flap side-edge.

f) Cut at 0.75 span-station

Figure 18: Comparison of computed pressure coefficients with the "QFF data"
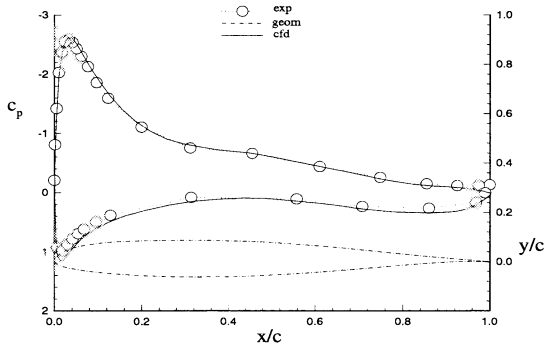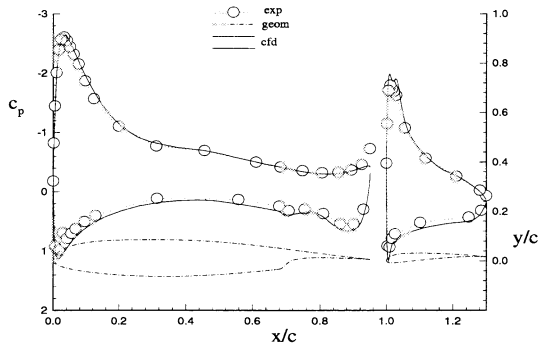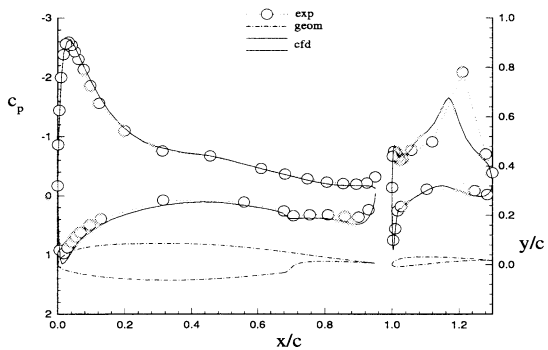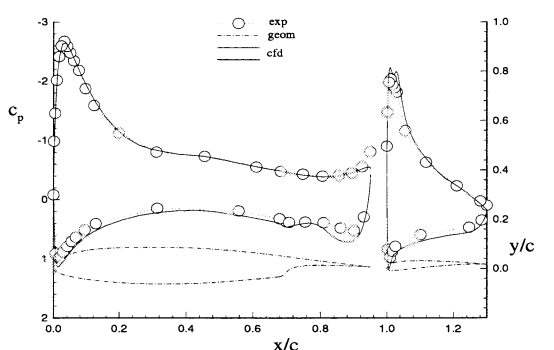$M=0.2$, $Re=1.8\times10^6$, $\alpha=16^\circ$, $\delta_f=29^\circ$